Quaternion structure of azimuthal instabilities

Giulio Ghirardo* and Mirko R. Bothien
Ansaldo Energia Switzerland, Baden 5401, Switzerland

(Received 17 February 2018; published 20 November 2018)

Rotationally symmetric systems can exhibit acoustic fluctuations in the azimuthal direction. In experimental works the nature (standing or spinning) of these fluctuations is often described by a set of indicators. These indicators either depend on the chosen frame of reference or are not state space variables for the acoustic field. Conversely, in theoretical works the field is projected on two orthogonal modes, and the system is characterized in terms of two amplitudes and one phase difference. Also in these works the nature of the field is not a state space variable but a derived quantity. Moreover the phase difference between the two modes is undetermined when one of the amplitudes of the two modes is zero, making the phase space ill-posed. We present a solution to these limitations, and we show how the acoustic field can be embedded in quaternion algebra, by calculating a suitable analytic signal of the complex-valued embedding of the acoustic field. This allows us to map the state of the system to a point that moves as function of time on a two-dimensional sphere in three-dimensional (3D) space, the Poincaré-Bloch sphere. To each state of the system corresponds just one point in this 3D space, which is then a well-posed phase space. We term the spherical coordinates of the point the amplitude of oscillation, the nature angle, and the orientation angle. The amplitude of oscillation of the system is the radius of the sphere. The nature angle is the latitude angle and positions the point closer to the equator (pure standing mode states) or closer to the poles (pure spinning mode states). The orientation angle is the longitude angle and describes the position of the pressure antinodes of the part of the acoustic field that is standing. These coordinates have a straightforward physical interpretation, can be easily calculated from experimental data, and are at the same time state space variables of a simple and elegant ansatz that can be used in low-order models. We also present an example of characterization of an experimental azimuthal thermoacoustic instability.

DOI: 10.1103/PhysRevFluids.3.113202

I. INTRODUCTION

Many combustion systems exhibit rotational symmetry, either full or discrete, around an axis of symmetry. For example, in the case of low-frequency azimuthal instabilities occurring in annular combustors the symmetry axis is the axis of the gas turbine rotor [1–3]. In the case of high-frequency, localized azimuthal instabilities the axis is often the axis of a burner or the axis of one can in can-annular combustors [4–6]. In both cases this symmetry can be exact or approximate [7–10]. In the exactly symmetric case some eigenmodes and eigenfrequencies of the system appear in pairs and have the same value (degenerate modes). In the approximate symmetric case the eigenfrequencies of the pairs are close (close to degenerate modes). We focus in this paper on one pair of degenerate or close to degenerate modes, which are solutions of the linearized problem and share approximately the same eigenfrequency.

*Corresponding author: giulio.ghirardo@ansaldoenergia.com

In the linear regime one can sum the two modes multiplied with arbitrary constants and still obtain a solution at only one frequency. Depending on the constants of this linear combination the whole acoustic field can be (1) a standing wave with pressure nodes and antinodes fixed in space, (2) a wave with nodes rotating in either counterclockwise or clockwise direction at the speed of sound, called the spinning wave by Crocco [11], or (3) a sum of a standing and a spinning wave. We refer to the standing or spinning nature of the acoustic field simply as the nature of the field in the following, and we will refer to the acoustic pressure simply as pressure. In the linear regime the nature of the acoustic field is undefined, because the coefficients can be chosen at will and lead to a different nature.

In the nonlinear regime, and in the absence of background noise or at low levels of noise, different factors push the system to settle for a certain nature, e.g., loss of symmetry [7,8], transverse forcing on the flame [12], or nonlinear saturation to axial forcing of the flame [13]. Here and in the following, we will use the term "flame" to refer to the fluctuating heat release rate response of the flame to the acoustic field.

For combustors exhibiting non-negligible levels of background noise we know that the solution is not deterministic anymore [14], and we currently do not have any theoretical prediction of the mode nature. Experimental works characterize the nature of the acoustic field with a set of indicators that we review in Sec. II. Theoretical studies project the governing equations on two orthogonal modes, which allow only an indirect calculation of the mode nature. This, and other shortcomings of orthogonal projections in a stochastic setting, are discussed in Sec. III. In Sec. IV we propose an ansatz such that the nature of the acoustic field is a state space variable. We make use of a quaternion valued analytic signal as proposed by Flamant *et al.* [15,16] and exploit a polar representation of a quaternion number as proposed by Bulow and Sommer [17]. The ansatz offers a simpler interpretation of the state of the system, either as an ellipse in the complex plane or as a point on a two-dimensional (2D) sphere in three-dimensional (3D) space. We draw links with other fields of science where these interpretations are well known. In Sec. V we apply the proposed ansatz to the analysis of an acoustic azimuthal instability of an industrial annular combustor. In Sec. VI we draw our conclusions.

II. REVIEW OF INDICATORS OF THE NATURE OF THE ACOUSTIC FIELD

The pressure field in cylindrical coordinates is $p(z, r, \theta)$ where z, r, θ are the axial, radial, and azimuthal coordinates, respectively, and we define the counterclockwise direction as the direction in which the azimuthal coordinate θ grows. Because the modes are of azimuthal type, we focus in the following only on the dependence of the pressure field on θ, by studying $p(\theta) \equiv p(\tilde{z}, \tilde{r}, \theta)$ with $\tilde{z}$ and $\tilde{r}$ fixed coordinates, e.g., the positions of the burners in an annular combustor. The theoretical investigation of Schuermans *et al.* [18] decomposes the pressure field for one dominant mode $p(\theta, t)$ in two orthogonal eigenmodes:

$$p(\theta, t) = \xi_1(t)\cos(n\theta) + \xi_2(t)\sin(n\theta), \tag{1}$$

where n is the order of the azimuthal mode considered, and $\cos(n\theta)$ and $\sin(n\theta)$ are the two orthogonal modes. This decomposition can be obtained, for example, from a truncation of a series expansion in cylindrical coordinates to the dominant terms [19,20]. The state of the system is determined by the amplitudes of the two oscillatory coefficients ξ_1, ξ_2 and the phase between them. We will reconsider orthogonal projections in Sec. III.

Schuermans proposed a so-called mode indicator, later used by Poinsot *et al.* [21] to classify the nature of the mode (standing or spinning) as a function of time for a short time series of an azimuthal instability. Worth and Dawson [22] apply a classification based on threshold values of the same indicator to classify the mode in standing and spinning. The indicator is defined as

$$C(t) = \frac{1}{N}\sum_m p_m(t) e^{in\theta_m}, \tag{2}$$

where $\{p_m(t) \equiv p(\theta_m, t),\ m = 1, \ldots, M_s\}$ are M_s pressure sensors positioned at the same axial location but at different azimuthal coordinates θ_m around the annulus and i is one of the two solutions of $i^2 = -1$. In the same work Worth and Dawson [22] also discuss how the ratio A_+/A_- of the amplitudes of the two counter-rotating waves is linked to the mode nature. The phase of the complex indicator C has a slope of $\pm\omega t$ for spinning waves and is constant for standing modes. This indicator has the shortcoming of not being valid if the pressure sensors p_m are not equispaced as detailed in Appendix A, as is often the case in industrial applications.

Bourgouin *et al.* [23] redefine the spin ratio to characterize the nature of the mode as

$$s \equiv \frac{A^+ - A^-}{A^+ + A^-}, \tag{3}$$

where A^+ and A^- are the slowly varying amplitudes of the two counter-rotating spinning waves that will be discussed later in Sec. III B. The spin ratio s equals ± 1 for spinning modes and 0 for standing modes. This indicator is a nonlinear function of the amplitudes $A^\pm$ and is independent of the angle of the chosen frame of reference. It differs from the original spin ratio proposed by Evesque *et al.* [24] because it allows one to distinguish between clockwise and counterclockwise spinning modes. More recently Refs. [25,26] also discuss the dynamics of an annular combustor based on the spin ratio defined in Eq. (3).

The indicator C presented in Eq. (2) and the spin ratio s presented in Eq. (3) are useful tools to understand azimuthal instabilities. They are, however, derived quantities, i.e., it is not straightforward to express the acoustic field p as a function of them as in $p(s)$ or $p(C)$. In particular, s in Eq. (3) depends nonlinearly on the amplitudes $A^+(t)$ and $A^-(t)$. The indicator C depends on the pressure field p, for which a suitable ansatz must be chosen in turn. These are not problems *per se* but make the validation of theoretical models cumbersome, as we discuss next first for the deterministic case, and then for the stochastic case. The orthogonal decomposition (1) suffers from other problems, discussed later in Sec. III.

In a deterministic framework, valid for systems exhibiting low levels of background noise, one can derive from the governing equations low-order dynamical systems [8,13,18] and quantitatively predict the solution. Then the indicators of this solution can be calculated and by comparing them with the experimental results one can assess the validity of the theory. For example, the theory of Ghirardo *et al.* [13] of rotationally symmetric annular combustors with a flame response depending only on the pressure has been validated against the Micca experiment equipped with perforated plates described in Ref. [27] by Ghirardo *et al.* [13] for the spinning case and by Laera *et al.* [28] for the standing case.

When one considers instead azimuthal instabilities with a non-negligible level of background noise, the prediction of the state of the stochastic system is necessarily probabilistic. In this case one aims to theoretically predict the probability density functions (PDFs) of the state variables of the dynamical system, which define the pressure field. Based on these PDFs one can predict the PDF of the indicator and compare it with the experimental PDF.

In both the deterministic and the stochastic case this comparison allows us to discuss the validity of the model only indirectly because the indicators are derived quantities. The main result of this work is to present a parametrization of the acoustic field that (1) is easy and fast to calculate, (2) does not depend on the frame of reference, (3) provides a good indicator for the standing or spinning nature, and (4) can be used as ansatz in low-order dynamical systems in a natural way. This allows us to directly compare model state variables with experimental values.

III. SHORTCOMINGS OF STUDYING AZIMUTHAL INSTABILITIES AS A SYNCHRONIZATION PROBLEM

This section discusses in Secs. III A and III B how to express the acoustic field as a linear combination of orthogonal modes, respectively, standing and spinning modes. We introduce the usage of the Hilbert transform and of the analytic signal and the concepts of slowly varying

amplitude and phase of each of the two oscillating modes, which will be needed in Sec. IV. In Secs. III C and III D we discuss some shortcomings that arise when the system is studied in terms of the amplitudes of the two modes and their phase difference.

A. Projection on two standing modes

The pressure field p appearing in Eq. (1) has two distinct timescales, a fast and a slow one. The fast timescale is one acoustic period $T = 2\pi/\omega$. Because thermoacoustics in gas turbines is typically only weakly nonlinear, in one period T the amount of acoustic energy added to the system by the flame, or taken from the system by the acoustic losses, is small. Then the amplitude A_m and the phase φ_m of each mode vary slowly as compared with the timescale T. One can write

$$\xi_m(t) = A_m(t)\cos[\omega t + \varphi_m(t)], \quad m = 1, 2, \tag{4}$$

where A_m and φ_m are real-valued quantities. By substituting (4) into (1) we obtain

$$p(\theta, t) = A_1(t)\cos[\omega t + \varphi_1(t)]\cos(n\theta) + A_2(t)\cos[\omega t + \varphi_2(t)]\sin(n\theta). \tag{5}$$

In low-order models of azimuthal instabilities one makes use of the ansatz (5) and of an additional constraint on (A_m, φ_m) to apply the method of averaging to the governing equations; see, e.g., Ref. [12]. One can introduce the phase difference

$$\tilde{\varphi}(t) \equiv \varphi_1(t) - \varphi_2(t) \tag{6}$$

describing the synchronization between the two standing modes. We review in Appendix B how if $A_1 = 0$ or $A_2 = 0$, or $\tilde{\varphi} = 0$ or $\tilde{\varphi} = \pi$ the system exhibits a standing wave, and how if $A_1 = A_2$ and $\tilde{\varphi} = \pm\pi/2$ the system exhibits a spinning wave, respectively, in the counterclockwise and clockwise direction. From an experimental perspective, the amplitudes A_m and the phase φ_m are estimated, respectively, as the modulus and slowly varying phase of the analytic signal of ξ_m [29–31]:

$$\xi_{\mathrm{a},m}(t) = A_m(t)e^{i[\omega t + \varphi_m(t)]}, \quad m = 1, 2. \tag{7}$$

The analytic signal $\xi_{\mathrm{a},m}$ appearing in Eq. (7) can be calculated from ξ_m as

$$\xi_{\mathrm{a},m}(t) = \xi_m(t) + \mathcal{H}[\xi_m](t)i, \quad m = 1, 2, \tag{8}$$

where $\mathcal{H}[\xi_m](t)$ is the Hilbert transform of $\xi_m(t)$. For reasons that will appear obvious later, we underline that the analytic signal $\xi_{\mathrm{a},m}$ is calculated along the i-imaginary axis because the Hilbert transform of the signal is added in Eq. (8) multiplied by the imaginary unit i. The ansatz (5) has been successfully used in low-order models [8,10,12–14,18], where the system is characterized in terms of the state space variables $\{A_1, A_2, \tilde{\varphi}\}$.

B. Projection on two spinning modes

One defines

$$\begin{aligned} 2\xi_{\mathrm{a}}^{+}(t) &\equiv \xi_{\mathrm{a},1}(t) + i\xi_{\mathrm{a},2}(t) \\ 2\xi_{\mathrm{a}}^{-}(t) &\equiv \xi_{\mathrm{a},1}(t) - i\xi_{\mathrm{a},2}(t) \end{aligned} \tag{9}$$

One proves by substitution that the pressure field (1) can be expressed as

$$2p(\theta, t) = \xi_{\mathrm{a}}^{+}(t)e^{-in\theta} + \xi_{\mathrm{a}}^{-}(t)e^{in\theta} + \text{c.c.}, \tag{10}$$

where c.c. denotes the complex conjugate of the quantity to its left. We now express $\xi_{\mathrm{a}}^{\pm}$ in terms of their slowly varying amplitude $A^{\pm}$ and phase $\varphi^{\pm}$, similarly to (7):

$$\xi_{\mathrm{a}}^{\pm}(t) = A^{\pm}(t)e^{i[\omega t + \varphi^{\pm}(t)]}. \tag{11}$$

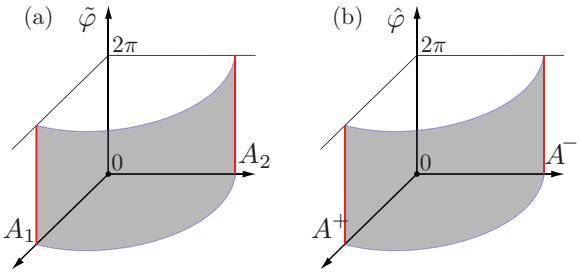

FIG. 1. (a) Phase space of the system in terms of the variables $\{A_1, A_2, \tilde{\varphi}\}$, employed when a projection on the two standing modes $\{\cos(n\theta), \sin(n\theta)\}$ is used. A_1 and A_2 are the positive amplitudes of the two standing modes, and the phase difference $\tilde{\varphi}$ between the two modes is periodic over $[0, 2\pi)$. The gray surface describes points at constant amplitude $\sqrt{A_1^2 + A_2^2}$. It can happen that the system state matches one of the two standing modes $\cos(n\theta)$, $\sin(n\theta)$, resulting in $A_2 = 0$ or $A_1 = 0$, respectively. In these cases, the system state is represented in phase space not by just one point, but by the left and right vertical red lines, respectively, because for these states the value of the phase difference $\tilde{\varphi}$ is undetermined. This makes the phase space ill-posed. (b) The same as for (a), but in terms of the variables $\{A^+, A^-, \hat{\varphi}\}$, employed when a projection on spinning modes is used. The same reasoning as for (a) applies.

By substituting (11) into (10) and dividing both sides by two we obtain

$$\begin{aligned} p(\theta, t) &= \frac{A^+}{2} e^{i\varphi^+} e^{i(\omega t - n\theta)} + \frac{A^-}{2} e^{i\varphi^-} e^{i(\omega t + n\theta)} + \text{c.c.} \\ &= A^+ \cos(\omega t - n\theta + \varphi^+) + A^- \cos(\omega t + n\theta + \varphi^-), \end{aligned} \tag{12}$$

where we dropped the explicit dependence on time of the variables A^+, A^-, φ^+, φ^-. Similarly to the case of the two standing modes, one can introduce the phase difference

$$\hat{\varphi}(t) \equiv \varphi^+(t) - \varphi^-(t) \tag{13}$$

describing the synchronization between the two spinning modes.

We observe from (12) that A^+ and A^- are the amplitudes of two spinning waves rotating, respectively, in the counterclockwise and clockwise direction, and then that ξ_a^+ and ξ_a^- defined in Eq. (9) are their respective analytic signals. The amplitudes A^+ and A^- appear in the definition (3) of the spin ratio. In particular (9) is the transformation between the orthogonal projections in terms of standing and spinning modes. The ansatz (10) has been successfully used in low-order models [32,33], where the system is characterized in terms of the state space variables $\{A^+, A^-, \hat{\varphi}\}$.

C. Shortcomings of using $\{A_1, A_2, \tilde{\varphi}\}$ as state space variables

Using a projection on two standing modes the state of the system is usually characterized in the 3D phase space of the slowly varying variables $\{A_1, A_2, \tilde{\varphi}\}$, as sketched in Fig. 1(a). It can happen that A_1 is zero and the pressure field in Eq. (5) is represented only by the mode with amplitude A_2. In this case the phase φ_1 is undetermined, and the variable $\tilde{\varphi}$ cannot be interpreted as the phase between two modes. In a deterministic framework, one can rotate the frame of reference of an angle such that that the two amplitudes A_1 and A_2 in the new frame of reference coincide and both modes are nonzero, as done in Ref. [13].

In a stochastic framework, the orientation of the acoustic field is random, and every choice of the frame of reference will lead to certain periods of time during which the amplitude of one of the two modes, say, A_1, is close to zero or zero. The amplitude A_1 and the phase φ_1 estimated by calculating the analytic signal of ξ_1 are affected by the level of background noise of the system. In particular if the amplitude A_1 is much larger than the noise level, then the signal ξ_1 has a clear sinusoidal shape on which the noise is added, and the reconstructed amplitude and phase of the

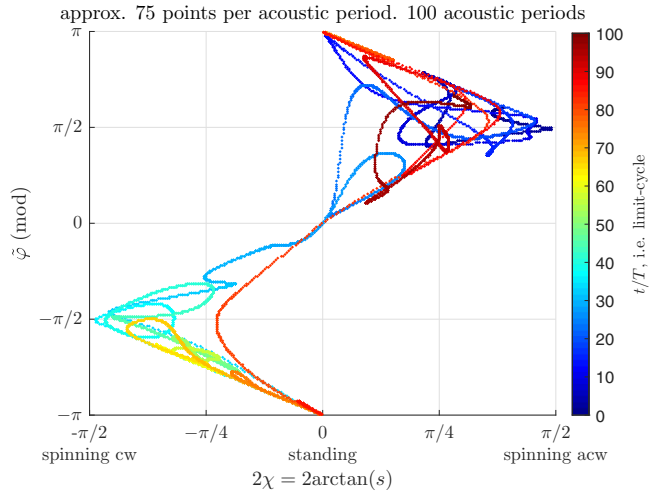

FIG. 2. Scatter chart for each instant of time of a thermoacoustic azimuthal instability. We plot on the horizontal axis a monotonic function of the the spin ratio s and on the vertical axis the phase $\tilde{\varphi}$ between two standing modes we decompose the pressure field, defined in Eq. (6). The color indicates the time. The two variables $\tilde{\varphi}$ and s are positively correlated, but $\tilde{\varphi}$ cannot be used instead of s or χ to describe the mode nature. The acronyms *acw* and *cw* stand for counterclockwise and clockwise.

instability are representative slowly varying quantities. If, instead, the amplitude A_1 is smaller or of the same order of the noise level the reconstructed phase φ_1 becomes a fast variable and is strongly perturbed by the noise (this is not the case for thermoacoustic instabilities of axial type where only one thermoacoustic mode oscillates, because the coherent oscillating behavior is usually stronger than the background noise level). This leads conversely to a fast variable $\tilde{\varphi}$ between the two modes. It follows that the variable $\tilde{\varphi}$ is representative of the state of the system when both amplitudes are far from zero, but loses meaning and is strongly affected by noise if one of the two amplitudes is close to zero, as depicted in Fig. 1(a). This is not a feature of the system dynamics but depends instead on the choice of the state space variables $\{A_1, A_2, \tilde{\varphi}\}$, which are the natural choice when employing a projection on orthogonal standing modes.

We also notice that only if we choose a frame of reference where at a certain instant of time $A_1 = A_2$, we can use the resulting phase difference $\tilde{\varphi}$ to infer the nature of the mode, as discussed after (6). In particular we present in Fig. 2 the relation between a monotonic function of the spin ratio s and the phase difference $\tilde{\varphi}$ for one case of an azimuthal instability in an annular combustor. We observe, for example, how if $s = 1$ then $\tilde{\varphi} = \pi/2$, the system spins counterclockwise and the nature of the acoustic field is well captured by both variables. However, the variable $\tilde{\varphi}$ is not a one-to-one mapping of the spin ratio s and then cannot be used as an indicator of the spinning or standing nature.

D. Shortcomings of using $\{A^+, A^-, \hat{\varphi}\}$ as state space variables

Using a projection on two spinning modes the state of the system is usually characterized in the 3D phase space of the slowly varying variables $\{A^+, A^-, \hat{\varphi}\}$, as sketched in Fig. 1(b). Also in this case it can happen that one of the two amplitudes, say, A^+, is zero or close to zero, leading to an undetermined phase difference $\hat{\varphi}$ between the two modes. While in the case of standing modes it is possible in principle to avoid this indeterminacy by rotating the frame of reference, in this case one can prove that the amplitudes A^+ and A^- are invariant under a rotation of the frame of reference and the value of A^+ would remain unchanged, not solving the indeterminacy of $\hat{\varphi}$. Regarding the nature of the acoustic field, the calculation of the spin ratio s using (3) is not affected by this indeterminacy

because it depends only on the two amplitudes A^+ and A^-. However, s is still a derived quantity of A^+ and A^- and not a state space variable itself.

This section illustrated how using $\{A_1, A_2, \tilde{\varphi}\}$ or $\{A^+, A^-, \hat{\varphi}\}$ as phase space variables leads in certain situations to the indeterminacy of the phase between the two orthogonal modes defining the projection basis. This is not a specific feature of azimuthal instabilities, but a general feature of the phase difference of two oscillators in 1:1 resonance when the amplitude of one of the two goes to zero. In the case of azimuthal instabilities, this happens when the system state matches exactly one of the two modes of the chosen basis (the two orthogonal standing modes or the two counter-rotating spinning modes respectively). This suggests that the study of azimuthal instabilities as a synchronization problem between two orthogonal modes is not ideal and prompts the search for a phase space that is not ill-posed. We have also reviewed how the nature of the acoustic field is not a state space variable but a derived quantity, harder to calculate in the phase space $\{A_1, A_2, \tilde{\varphi}\}$ than in the phase space $\{A^+, A^-, \hat{\varphi}\}$.

Despite these shortcomings, the state space variables $\{A_1, A_2, \tilde{\varphi}\}$ or $\{A^+, A^-, \hat{\varphi}\}$ have been extensively used in the literature. They can be extracted easily from experimental data and allow the simple ansatz (5) and (12) for low-order models. In the next section we propose a new ansatz such that the mode nature is a state space variable and there is a representation of the state of the system that is well-posed.

IV. AMPLITUDE, NATURE, AND ORIENTATION OF THE ACOUSTIC FIELD

This section shows how azimuthal instabilities can be studied in the context of quaternion algebra. Quaternion numbers were discovered by Hamilton [34] and comprise three imaginary units instead of one imaginary unit as in the case of complex numbers. They will be introduced later where needed. In Sec. IV A we present how quaternion algebra is a viable approach to the problem. In Sec. IV B we discuss the physical interpretation and draw links to other fields of science where this type of analysis is standard. We stress that quaternion algebra is a tool with which we discover the ansatz, but the ansatz is real-valued and holds regardless of quaternion algebra.

A. The analytic signal

We would like to find a way of characterizing the acoustic field that is robust and determined with respect to a change of the frame of reference and to situations where the acoustic field is in a pure spinning or standing state. We recognize that the two signals $\{\xi_1(t), \xi_2(t)\}$ are just one of the many couples of signals observed from a different frame of reference and could then be treated as a bivariate signal. We define

$$\xi(t) \equiv \xi_1(t) + i\xi_2(t) \tag{14}$$

so that we can express the pressure field (1) as

$$2p(\theta, t) = e^{-in\theta}\xi(t) + \text{c.c.} \tag{15}$$

The variable ξ in Eq. (14) is the complex embedding of the bivariate signal (ξ_1, ξ_2), as commonly used, e.g., by Gonella [35] or discussed in the introduction of the book of Schreier and Scharf [36]. It allows us to write the pressure field in terms of one variable only, ξ. We now proceed similarly to how we treated each of the two modes in the previous subsection. In particular, we would like to express the slowly varying components of (14) similarly to how it is done in Eqs. (7) and (8), by means of the Hilbert transform and the concept of analytic signal. We point out next, however, how this is not trivial.

We observe from (8) that the analytic signals of the two parts of ξ are

$$\begin{aligned}\xi_{\text{a},1}(t) &= \xi_1(t) + i\mathcal{H}[\xi_1](t)\\ \xi_{\text{a},2}(t) &= \xi_2(t) + i\mathcal{H}[\xi_2](t).\end{aligned} \tag{16}$$

If we were to define the analytic signal of ξ as $\xi_a \equiv \xi_{a,1} + i\xi_{a,2}$ the two signals would mix together, i.e., we would obtain

$$\{\xi_1(t) - \mathcal{H}[\xi_2](t)\} + i\{\mathcal{H}[\xi_1](t) + \xi_2(t)\}, \tag{17}$$

which is twice the analytic signal of the spinning mode ξ_a^+ presented in Eq. (9), and cannot then be interpreted as the analytic signal of the whole ξ. One is also tempted to define the analytic signal of ξ as $\xi + i\mathcal{H}[\xi]$, but this option leads to an expression that we cannot make physical sense of.

We propose instead to introduce an additional imaginary unit j. We calculate separately the analytic signals of the real and imaginary parts of ξ along the j axis:

$$\begin{aligned}\xi_{a,1}(t) &\equiv \xi_1(t) + j\mathcal{H}[\xi_1](t)\\ \xi_{a,2}(t) &\equiv \xi_2(t) + j\mathcal{H}[\xi_2](t).\end{aligned} \tag{18}$$

Also in this case we can express the analytic signals in terms of slowly varying amplitudes and phases:

$$\xi_{a,m}(t) = A_m(t)e^{j[\omega t + \varphi_m(t)]}, \quad m = 1, 2, \tag{19}$$

where the expression (19) differs from (7) only because of the choice of the imaginary unit j instead of i, and we will elucidate how j differs from i later. We define the analytic signal of ξ as

$$\xi_a(t) \equiv \xi_{a,1}(t) + i\xi_{a,2}(t) \tag{20a}$$

$$= \xi_1(t) + j\mathcal{H}[\xi_1](t) + i\{\xi_2(t) + j\mathcal{H}[\xi_2](t)\}. \tag{20b}$$

In a manner that we will show later to be fully equivalent to the definitions (20) and (18), one can define the analytic signal $\xi_a(t)$ as

$$\xi_a(t) \equiv \xi(t) + \mathcal{H}[\xi](t)j. \tag{21}$$

The proposed definition (21) of the analytic signal of a complex-valued signal ξ differs from the real-valued case presented in Eq. (8) just by the choice of a different imaginary unit in the definition.

By introducing the additional imaginary unit j, we have left open to interpretation the meaning of the presented mathematical expressions until we discuss which algebra we are using. We choose the associative noncommutative algebra of quaternions. An introduction to quaternion algebra can be found in the book of Doran and Lasenby [37], but we discuss here all the properties of quaternions needed in this paper. In quaternion algebra there are three imaginary units $\{i, j, k\}$ such that $i^2 = j^2 = k^2 = -1$ and that $ij = k,\ jk = i,\ ki = j$. By using the rule $ij = k$ we simplify (20):

$$\xi_a(t) \equiv \xi_1(t) + i\xi_2(t) + j\mathcal{H}[\xi_1](t) + k\mathcal{H}[\xi_2](t). \tag{22}$$

In a similar manner one obtains (22) from (21). We recover the analytic signal of the first mode in the real and j-imaginary components of (22) and the analytic signal of the second mode in the i- and k-imaginary components. The original complex-valued signal ξ is simply

$$\xi(t) = \mathrm{Re}[\xi_a(t)] + i\,\mathrm{Im}_i[\xi_a(t)]. \tag{23}$$

A slightly different definition of the analytic signal $\xi_a(t)$ of a complex-valued signal $\xi(t)$ was proposed by Le Bihan *et al.* [38] and named the hypercomplex signal. In later publications [15,16] the definition (21) was proposed by the same authors, with the name quaternion embedding of the complex-valued signal ξ. We will instead call ξ_a the analytic signal of ξ because, in the same way as the real-valued case, it maps a time series with one fast oscillating component to a time series where slowly varying quantities are defined, as we discuss next [also because the term "embedding" usually means something else, as discussed after (14)].

From a practical perspective, we observe that the four real-valued components of the signal ξ_a in Eq. (22) can be calculated separately using real-valued algebra. By direct substitution of (19) into

(20a) we can express $\xi_a(t)$ in terms of the slowly varying amplitudes and phases of the two modes:

$$\xi_a(t) = [A_1(t)e^{j\varphi_1(t)} + iA_2(t)e^{j\varphi_2(t)}]e^{j\omega t}. \tag{24}$$

Given a quaternion number $a + ib + jc + kd$ with $\{a, b, c, d\} \in \mathbb{R}^4$, its quaternion conjugate is $a - ib - jc - kd$. We can express the pressure field $p(\theta, t)$ in Eq. (1) in terms of $\xi_a(t)$ and its quaternion conjugate:

$$2p(\theta, t) = e^{-in\theta}\xi_a(t) + \text{q.c.} = 2\text{Re}[e^{-in\theta}\xi_a(t)], \tag{25}$$

where q.c. denotes the quaternion conjugate of the quantity to its left. The modulus of a quaternion number $a + ib + jc + kd$ is simply $\sqrt{a^2 + b^2 + c^2 + d^2}$. We can introduce the amplitude A as the modulus of the analytic signal ξ_a:

$$A \equiv |\xi_a| = \sqrt{\xi_1^2 + \mathcal{H}[\xi_1]^2 + \xi_2^2 + \mathcal{H}[\xi_2]^2} = \sqrt{A_1^2 + A_2^2} = \sqrt{2(A^+)^2 + 2(A^-)^2}. \tag{26}$$

One advantage of ξ_a in Eq. (22) as compared to the two separate analytic signals $\xi_{a,m}(t)$ for $m = 1, 2$ presented in Eq. (8) is that the amplitude A does not go to zero when one of A_1 or A_2 goes to zero individually, which is one feature of the problem reviewed in Sec. III. It is unclear at this stage, however, how the expressions (22) and (25) can help to characterize standing and spinning modes, which is the focus of the next section.

B. Interpretation of the analytic signal

Every nonzero quaternion, and then for our application the quaternion ξ_a in Eq. (22), can be expressed as

$$\xi_a(t) = A(t)e^{in\theta_0(t)}e^{-k\chi(t)}e^{j[\omega t+\varphi(t)]} \tag{27}$$

with $A \in (0, \infty)$, $n\theta_0 \in (-\pi, \pi]$, $\chi \in [-\pi/4, \pi/4]$, $\varphi \in (-\pi, \pi]$, and we stress that φ does not have a tilde or a hat to differentiate it from $\tilde{\varphi}$ defined in Eq. (6) and from $\hat{\varphi}$ defined in Eq. (13). The structure (27) parametrizes a general quaternion in terms of the amplitude $A(t)$ of oscillation and the three angles $n\theta_0(t)$, $\chi(t)$, and $\omega t + \varphi(t)$. In our application only the last angle $\omega t + \varphi(t)$ is a fast varying quantity. The decomposition (27) in a slightly different form was discussed first by Bulow and Sommer [17]. The calculation of the four variables $\{A, \chi, n\theta_0, \omega t + \varphi\}$ from the quaternion ξ_a is detailed in Appendix C. This section discusses the interpretation and physical meaning of the slowly varying variables A, χ, θ_0, and φ from different perspectives.

1. The pressure field

By substituting (27) into (25) we obtain

$$\begin{aligned} 2p(\theta, t) &= Ae^{in(-\theta+\theta_0)}e^{-k\chi}e^{j(\omega t+\varphi)} + \text{q.c.} \\ &= [A\cos[n(-\theta + \theta_0)]\cos(\chi)\cos(\omega t + \varphi) \\ &\quad + ikjA\sin[n(\theta - \theta_0)]\sin(\chi)\sin(\omega t + \varphi) + \text{other imaginary terms}] + \text{q.c.} \qquad (28) \\ &= 2A\cos[n(\theta - \theta_0)]\cos(\chi)\cos(\omega t + \varphi) + 2A\sin[n(\theta - \theta_0)]\sin(\chi)\sin(\omega t + \varphi), \qquad (29) \end{aligned}$$

where in the second passage we exploit the fact that the product of the quaternion imaginary units is anticommutative, so that $ik = -ki = -j$ and then $ikj = -jj = 1$. We discuss next the three angles χ, θ_0, φ.

The nature angle: If we substitute $\chi = \pi/4$ in Eq. (29) we obtain

$$\begin{aligned} 2p(\theta, t) &= +\sqrt{2}A\cos[n(\theta - \theta_0)]\cos(\omega t + \varphi) + \sqrt{2}A\sin[n(\theta - \theta_0)]\sin(\omega t + \varphi) \qquad (30) \\ &= +\sqrt{2}A\cos[\omega t + \varphi - n(\theta - \theta_0)]. \qquad (31) \end{aligned}$$

From (31) we observe that for $\chi = \pi/4$ the system exhibits a spinning wave rotating in the direction of a growing azimuthal coordinate θ, i.e., in the counterclockwise direction; conversely $\chi = -\pi/4$ corresponds to a spinning wave rotating in the clockwise direction. If we substitute $\chi = 0$ we obtain a standing wave, regardless of the values of the other parameters A, θ_0, φ. We then propose to call χ the nature angle, because it determines the spinning or standing nature of the acoustic field. A positive nature angle χ corresponds in the general case to a sum of standing and spinning modes where the spinning component rotates in the counterclockwise direction, i.e., the pressure antinodes of such component move at the speed of sound in the positive θ direction. Conversely $\chi < 0$ corresponds to modes whose spinning component rotates in the clockwise direction. We prove in Appendix D that the following relation holds between the spin ratio defined in Eq. (3) and the nature angle:

$$s = \tan \chi. \tag{32}$$

The orientation angle: For $\chi = 0$ the pressure field (29) simplifies to

$$2p(\theta, t) = +2A \cos[n(\theta - \theta_0)] \cos(\chi) \cos(\omega t + \varphi). \tag{33}$$

Equation (33) shows that the angle θ_0 determines the location of the pressure antinodes of the resulting standing wave, and we then call it the orientation angle. This angle holds the same interpretation also for pressure fields partially standing and partially spinning. For example, for $\chi \in (0, \pi/4)$ we introduce $\Delta \equiv A \cos \chi$ and $\delta \equiv A \sin \chi$, with $\Delta > \delta > 0$. By substituting these expressions in Eq. (29) we obtain

$$\begin{aligned} p(\theta, t) &= +(\Delta - \delta) \cos[n(\theta - \theta_0)] \cos(\omega t + \varphi) \\ &\quad + \delta[\cos[n(\theta - \theta_0)] \cos(\omega t + \varphi) + \sin[n(\theta - \theta_0)] \sin(\omega t + \varphi)] \qquad (34) \\ &= +(\Delta - \delta) \cos[n(\theta - \theta_0)] \cos(\omega t + \varphi) + \delta \cos[\omega t + \varphi - n(\theta - \theta_0)]. \qquad (35) \end{aligned}$$

In Eq. (35) the pressure field consists of a standing component (first term) and a spinning component (second term). In Eq. (35) the azimuthal location with the maximum value of the pressure in the span of one limit cycle [39] is θ_0, which is also the angle of the pressure antinodes of the standing component.

We observe that the orientation angle $n\theta_0$ is a slowly varying variable and cannot be linked with the azimuthal position of the nodal line calculated in Ref. [27], which is a fast varying variable and for a pure spinning mode rotates around the annulus at the speed of sound. We prove in Appendix E that the orientation angle matches the phase $\hat{\varphi}/2$. It also seems to match, apart for multiplicative terms, the so-called nondimensional position of the standing wave discussed in Ref. [22].

The phase: Finally, the angle φ is the only slowly varying angle in the time coordinate, and hence we call it simply the slowly varying phase of the system, typical of oscillatory systems studied in polar coordinates [40,41] and different from the phase difference $\tilde{\varphi}$ and $\hat{\varphi}$ introduced in Eqs. (6) and (13).

The physical interpretation of the four variables $A, \theta_0, \chi, \varphi$ presented in this section depends on the fact that the pressure field $p(\theta, t)$ is $e^{-in\theta}/2$ times the analytic signal $\xi_a(t)$ as detailed in Eq. (25). This specific expression of the pressure p in terms of the analytic signal depends on the application considered, which in our case is acoustics. In the next two sections we discuss interpretations of the four variables that are more general and based only on the structure of (27). We also discuss other applications where the same four variables describe different physics.

2. Ellipse in the complex plane

In this section we discuss the path of the 2D point $(\xi_1(t), \xi_2(t))$ in the (ξ_1, ξ_2) plane, i.e., the path of the complex-valued point $\xi(t)$ introduced in Eq. (23) in the complex plane. By substituting (27) into (23) we obtain

$$\xi = Ae^{in\theta_0}[\cos \chi \cos(\omega t + \varphi) + i \sin \chi \sin(\omega t + \varphi)] \tag{36}$$

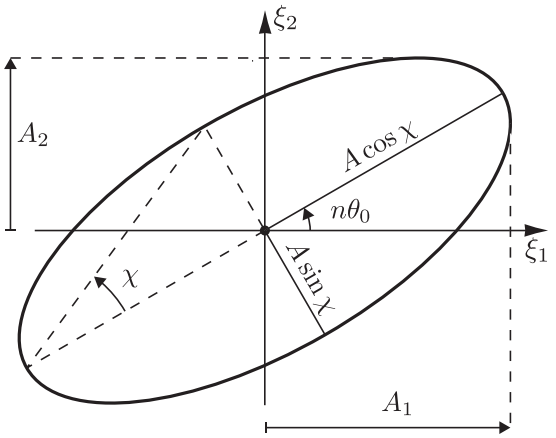

FIG. 3. The system has two timescales. On the fast timescale of the period of the thermoacoustic oscillation the point $\xi_1(t) + i\xi_2(t)$ rotates in the complex plane around the origin and draws one ellipse for each period. On the slow timescale the parameters A, χ, and θ_0 slowly change the shape of the ellipse. In particular the nature angle χ determines whether the ellipse collapses to a line (standing state) or to a circle (spinning state), while the angle θ_0 sets the inclination of the ellipse with respect to the axis ξ_1 and the orientation of the standing component of the acoustic field. For $\chi > 0$ the point moves in the counterclockwise direction on the ellipse, while for $\chi < 0$ it moves clockwise.

Equation (36) matches [42] the definition of the modulated elliptical signal as presented e.g., by Lilly *et al.* [43,44]. In particular the expression (36) traces in the complex plane an ellipse, with major axis of length $A\cos\chi$, minor axis of length $A\sin\chi$, and angle $n\theta_0$ between the major axis of the ellipse and the real axis, as presented in Fig. 3. The term *modulated* here characterizes the fact that while the fast timescale of the phase ωt traces the ellipse, the slow variables A, $n\theta_0$, and χ slowly deform its scale, orientation, and ellipticity.

For $\chi = \pm\pi/4$ the ellipse is a round circle, with the point traveling on the circle, respectively, in the counterclockwise or clockwise direction. These special circular cases represent spinning waves in the counterclockwise or clockwise direction, and for them the orientation angle θ_0 is meaningless. For $\chi = 0$ the ellipse collapses to a line, which forms an angle θ_0 with the real axis. This special line cases represent standing waves. We dedicate the rest of this section to show how this ellipse is common in two other fields of science.

The shape of the ellipse traced in the complex plane dates back at least to the work in Refs. [35,45] in oceanographic currents analysis, where the flow field is discussed in terms of rotary currents (clockwise and counterclockwise).

In optics the (x, y) components (E_x, E_y) of the electric field $\boldsymbol{E}$ of a beam of light traveling in the z direction draw an ellipse in the (x, y) plane, called the polarization ellipse. One typically works with the vector proposed by Jones [46], defined as

$$\boldsymbol{A}_J \equiv \begin{bmatrix} A_1 e^{i\varphi_1} \\ A_2 e^{i\varphi_2} \end{bmatrix} \tag{37}$$

and called the Jones vector, where the subscripts 1 and 2 refer to the x and y directions, respectively. The x and y components of the electric field are $\mathrm{Re}[\boldsymbol{A}_J e^{i(k_z z - \omega t)}]$ where k_z is the wave number in the z direction and the z component is trivially zero. These two components of $\boldsymbol{A}_J$ appear in the first factor at the right-hand side of (24). The case of the ellipse matching a perfect circle is referred to as circular polarized state. The case of a line is referred to as linear polarized state in the $n\theta_0$ direction. All other possible states are classified as elliptically polarized states. The polarization ellipse is fully determined by A, χ, and $n\theta_0$ and does not depend on the frame of reference. In particular A and

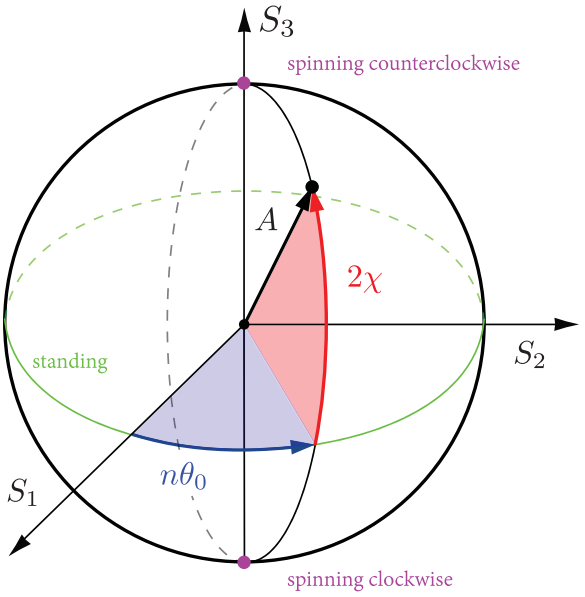

FIG. 4. Sketch of the Poincaré sphere. Points on the equator represent pure standing waves. The north and south poles represent waves spinning, respectively, in the counterclockwise and clockwise direction. To each state of the system corresponds only one point in this 3D space.

χ are invariant quantities, and θ_0 is a covariant quantity with respect to a rotation of the frame of reference.

3. Poincaré-Bloch sphere

Poincaré [47] was the first to observe in the study of light polarization that the variables $\{A, 2\chi, n\theta_0\}$ span $(0, \infty) \times [-\pi/2, \pi/2] \times [-\pi, \pi]$ and can then be interpreted as spherical coordinates in a 3D space, as presented in Fig. 4. In particular A is the radius of the sphere, 2χ is the latitude angle, and $n\theta_0$ is the longitude angle [48]. Dynamics of the system involving a change of amplitude occur in the direction of the sphere radius. Dynamics involving a change of mode nature, from standing to spinning or vice versa, occur in the north-south direction. Dynamics involving a change of orientation of the part of the acoustic field that is standing occur in the east-west direction. A system dominantly spinning lingers close to the poles, while a system dominantly standing lingers close to the equator.

An appealing property of the Poincaré-Bloch sphere representation is that each state of the system is mapped exactly to one point, and conversely that each point on the sphere corresponds to only one state of the system. This means that a trajectory of the system as a function of time in the 3D space of Fig. 4 is robust against noise and does not suffer from the indeterminacy occurring to the phase variables $\tilde{\varphi}$ and $\hat{\varphi}$ discussed in Sec. III. We point out that this occurs when using as phase space the 3D coordinates $\{S_1, S_2, S_3\}$ of Fig. 4 generated by interpreting $\{A, 2\chi, n\theta_0\}$ as spherical coordinates, and not in terms of the coordinates $\{A, 2\chi, n\theta_0\}$ themselves [49].

We refer the reader to the book by Holm [50, Sec. 4.1] for a related theoretical, geometric view on the role of the Poincaré sphere on pairs of resonant oscillators. In quantum mechanics the Poincaré sphere is called the Bloch sphere and is used [51] to study two-state quantum systems [52]. One example of a two-state system is a particle on a circle, governed by the Schrödinger equation on a periodic domain, as reviewed, e.g., by Lowe and Peterson [53, Sec. 2-6]. The corresponding

eigenvalue problem presents degenerate pairs of eigensolutions, in the same way as the wave equation in a circular domain considered in this paper if rotational symmetry is assumed.

This section has presented how the ellipse parameters and/or the spherical coordinates on the Poincaré-Bloch sphere describe as functions of time the state of the system. We have made use of quaternion algebra to recover these quantities, but we point out here that one can calculate the same quantities without quaternion algebra, as presented, e.g., by Schreier *et al.* [54] and Lilly *et al.* [44]. The two approaches are compared by Le Bihan *et al.* [38, Sec. 6]. Other ways of estimating the position on the Poincaré-Bloch sphere have been proposed too; see, e.g., Refs. [55,56].

V. REAL-WORLD EXAMPLE

Prompted by one reviewer, we add in this section an application that should clarify the physical interpretation of the proposed quantities. We consider the azimuthal combustion instability presented in Ref. [10], before and after the installation of a set of acoustic dampers around the annulus. These dampers are implemented to widen the gas turbine operation window by reducing combustor pulsations induced by thermoacoustic phenomena. We discuss in Sec. V A a time domain analysis of a small observation window. Then we discuss the statistics of a longer observation window in terms of marginal probability density functions in Sec. V B and in terms of joint probability density functions in Sec. V C.

A. Time domain

We present in Fig. 5 the time domain evolution of the maximum amplitude of 100 limit cycle oscillations of the azimuthal instability before the dampers installation. We study them in terms of standing modes in Fig. 5(a), in terms of spinning modes in Fig. 5(b), and with the new quaternion projection in Fig. 5(c). In the three subfigures the horizontal time axis is shared, the amplitudes are measured on the left vertical scale and angles and phases on the right vertical scale. One recognizes, for example, in Fig. 5(a) at time $t \approx 22T$ how the fact that the phase $\tilde{\phi}$ suddenly jumps value is just a limitation of the chosen orthogonal projection on standing modes. It happens because one of the two amplitudes becomes very small, and it does not correspond to any particular physical state of the system. The same happens in Fig. 5(b) at time $t \approx 9T$ for the projection on spinning modes, exemplifying how the two sets of variables $\{A_1, A_2, \tilde{\varphi}\}$ and $\{A^+, A^-, \hat{\varphi}\}$ of these two projections do not carry physical meaning in all their phase space. The proposed quaternion projection, presented in Fig. 5(c), characterizes the state of the system in terms of the amplitude A, the nature angle χ, and the azimuthal orientation angle $n\theta_0$ of the standing component of the pressure field, which are all physical quantities. At time $t \approx 22T$ it shows that the system state is close to a standing mode because 2χ is close to zero, with an orientation angle $n\theta_0$ that is increasing. At time $t \approx 9T$ the system state nature 2χ changes very quickly, and the azimuthal angle $n\theta_0$ undergoes a fast change. This is, however, physical and not an artifact of the proposed projection. The standing component of the pressure field has a very small amplitude, and little dynamics can strongly affect its orientation as observed in this case.

We showed in the previous section that $n\theta_0$ and χ, together with the proposed amplitude A, are not just observables of the system state, but fully describe it, i.e., are valid state space variables. From an experimental perspective, this means that in order to to characterize the system, we can look at these variables only. We present steady state statistics in terms of these variables next.

B. Marginal probability density functions

We present on the diagonal of Fig. 6 the marginal probability density functions (PDFs) of each of the three variables $\{A, 2\chi, n\theta_0\}$ for an observation time of approximately 19 000 limit cycles. We characterize the system before the installation of the dampers (red) and after the installation of the dampers (black). The amplitude A is nondimensionalized in terms of the mean amplitude $\overline{A}$ before dampers' installation.

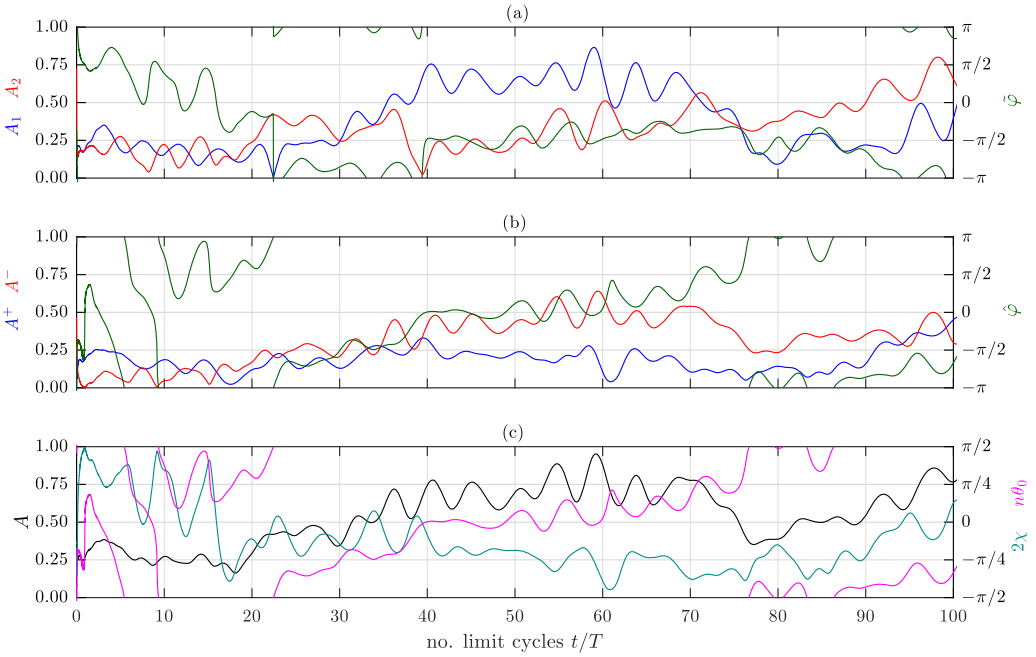

FIG. 5. Characterization of 100 acoustic periods of an azimuthal instability, in terms of (a) the amplitudes A_1, A_2 (blue and red, left axis) of two standing modes and their phase difference $\tilde{\phi}$ (green, right axis); (b) the amplitudes A^+, A^- of two counter-rotating spinning(rotating) modes (blue and red, left axis) and their phase difference $\hat{\phi}$ (green, right axis); (c) the amplitude A of the whole field (black, left axis), the nature angle χ describing if the field is rotating or standing (blue green, right axis), and the orientation angle $n\theta_0$ of the part of the field that is standing (magenta, right axis). The three representations are mathematically equivalent because they fully describe the state of the system. Only (c) casts the system state in terms of physically meaningful variables at all times. The ill-posedness of the phase space in terms of standing modes can be observed for example at $t \approx 22T$ where the phase $\tilde{\phi}$ abruptly jumps, and similarly in (b) at $t \approx 9T$. (a) projection on standing modes, (b) projection on spinning modes, and (c) proposed projection.

In Fig. 6(a) we observe that the installation of the dampers led to a significant reduction of the amplitude of oscillation. In Fig. 6(e) we observe that the most likely nature angle 2χ before dampers' installation is between 0 and $\pi/4$, while after dampers' installation the peak shifts to 0. In both cases the pure spinning states, i.e., the values of $\pm\pi/2$, are not very likely. In Fig. 6(i) we observe that the orientation angle before the installation of the dampers (red) has a marginal PDF that is in a first rough approximation flat, with all angles having approximately the same probability. After the installation of the dampers, the probability of the orientation angle $n\theta_0$ of the standing component, which is also the orientation of the maximum of the acoustic pressure, is close to 0.

C. Joint probability density functions

We present in the off-diagonal subfigures of Fig. 6 the joint PDFs of two variables at a time [57]. Couples of subfigures that are symmetric with respect to the diagonal represent the same quantities respectively before (subfigures above the diagonal, red shades) and after (subfigures below the diagonal, gray shades) the installation of the dampers.

In Figs. 6(b) and 6(d) we observe that the probability density function $P(2\chi, A/\overline{A})$ has a clear peak and seems to be factorable.

We observe in Figs. 6(c) and 6(g) how at low amplitudes the values of the orientation angle are equally likely, because the contour lines are approximately flat. This is consistent with the theory,

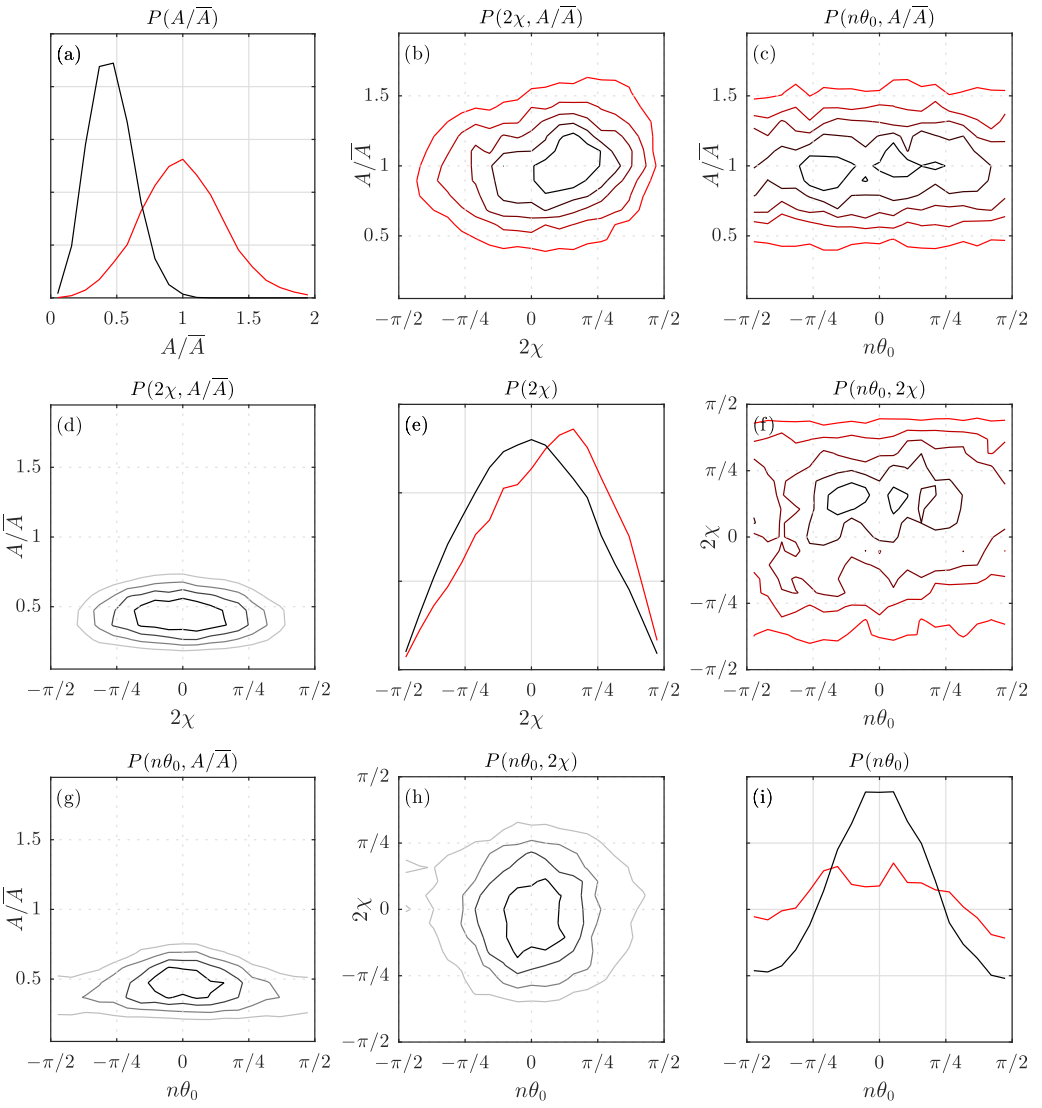

FIG. 6. Characterization of approximately 19 000 acoustic periods of an azimuthal combustion instability in terms of marginal probability density functions (PDFs, subfigures on the diagonal) and joint PDFs (off-diagonal subfigures). Red shades correspond to time series measured before the installation of the acoustic dampers, and black shades correspond to time series measured after their installation. The installation of the dampers leads to (a) a reduction of the amplitude of pulsation A; (e) a shift of the nature angle 2χ towards a standing state; (i) a preference for an orientation angle around 0 of the standing component.

which predicts that in the linear regime the two modes [58] are decoupled, from which it follows that the orientation angle is random, with each value being equally likely.

We expect that if the system state is almost completely spinning, the orientation angle $n\theta_0$ should be strongly affected by the background noise and then have an approximately uniform probability function. This is the case before the installation of the dampers in Fig. 6(f), where we observe that the contour lines close to $2\chi = \pm\pi/2$ are approximately flat. This is harder to characterize after the installation of the dampers, because the system lingers for most of the time closer to a standing state, and only for a minority of time close to a spinning state where the orientation angle is undetermined.

Still, we observe in Fig. 6(h) that the conditional PDF $P(n\theta_0|2\chi = 2\chi^\star)$ for a given value of the angle $2\chi^\star$ broadens as $2\chi^\star$ departs from 0.

VI. CONCLUSIONS

We show how existing indicators of the nature (standing or spinning) of azimuthal instabilities are not optimal because they are derived quantities of the acoustic field and cannot be directly used as state space variables. We show how orthogonal projections offer convenient state space variables but allow the calculation of the mode nature only indirectly, and these variables determine an ill-posed phase space. We make use of quaternion algebra, which is equipped with three imaginary units i, j, k, to find an ansatz that solves these shortcomings. We propose a new ansatz for an azimuthal acoustic pressure field oscillating at an angular frequency ω in Eqs. (25) and (27), which can be combined to obtain

$$2p(\theta, t) = A(t)e^{in[\theta_0(t)-\theta]}e^{-k\,\chi(t)}e^{j[\omega t+\varphi(t)]} + \text{q.c.}, \tag{38}$$

where q.c. denotes the quaternion conjugate of the term to its left. Equation (38) evaluates to the real-valued solution (29):

$$2p(\theta, t) = 2A\cos[n(\theta-\theta_0)]\cos(\chi)\cos(\omega t+\varphi) + 2A\sin[n(\theta-\theta_0)]\sin(\chi)\sin(\omega t+\varphi). \tag{39}$$

We identify in Eqs. (38) and (39) four state space variables that have a direct physical interpretation:

(1) The amplitude A of the acoustic field

(2) The orientation angle $n\theta_0$, describing the orientation of the standing component of the acoustic field; one can characterize the mean azimuthal flow velocity by studying the mean drift of the orientation angle θ_0, if any

(3) The nature angle χ, quantifying how much the system is standing and/or spinning, and in which direction it spins

(4) The slowly varying phase φ of oscillation.

These four state space variables $\{A, \chi, n\theta_0, \varphi\}$ can be reconstructed from experimental or numerical time series of the acoustic field and can be used in low-order models, allowing a direct validation of theoretical results. We provide in Sec. V an experimental example of application of these concepts on the time series of an acoustic azimuthal instability of an industrial annular combustor. We find a link between the nature angle χ and the spin ratio s proposed by Bourgouin *et al.* [23], and in particular we prove that $s = \tan\chi$.

The proposed ansatz allows two geometrical representations of the state of the system: the polarization ellipse of Fig. 3 and the Poincaré-Bloch sphere of Fig. 4. We review how both representations are used in other fields of physics that share a similar mathematical structure, e.g., light polarization, wind and oceanic 2D currents, and two-state quantum systems. When the system lingers in the vicinity of a purely spinning state, the angle $n\theta_0$ is undetermined, or strongly perturbed by the noise. A robust way to represent and compare predictions and experimental results is to characterize the state of the system on the Poincaré sphere, where the indeterminacy of $n\theta_0$ does not propagate.

The new ansatz leads also to a change of perspective: existing theoretical works on azimuthal instabilities make use of orthogonal projections and study the resulting solutions as synchronization states between the two oscillatory orthogonal modes. This, however, has the shortcoming that when one of the two modes has a zero amplitude the synchronization phase is undetermined and loses physical meaning. With the newly proposed ansatz the nature of the acoustic field is instead the state space variable χ.

The results apply both to low-frequency azimuthal instabilities typical of annular combustors, either rotationally symmetric or not, and to high-frequency azimuthal thermoacoustic modes localized in space and close to eigenfrequency degeneracy. A similar approach may be useful to

study oscillations in other rotationally symmetric problems, e.g., the wake behind a symmetric bluff body [59,60].

APPENDIX A: DEPENDENCE OF $C(T)$ ON THE FRAME OF REFERENCE

We consider for convenience the case $n = 1$, and split (2) into real and imaginary parts:

$$C(t) = \frac{1}{N}\sum_m p(\theta_m, t)\cos(\theta_m) + i\frac{1}{N}\sum_m p(\theta_m, t)\sin(\theta_m). \tag{A1}$$

We consider the standard orthogonal decomposition of the pressure field (1), and substitute it into (A1). We obtain

$$\begin{aligned} C(t) = \frac{1}{N}\Bigg\{&\left[\sum_m \xi_1 \cos^2(\theta_m) + \sum_m \xi_1 \sin(\theta_m)\cos(\theta_m)\right] \\ &+ i\left[\sum_m \xi_2 \sin^2(\theta_m) + \sum_m \xi_2 \sin(\theta_m)\cos(\theta_m)\right]\Bigg\}. \end{aligned} \tag{A2}$$

If the pressure sensors are equispaced we have that

$$\begin{aligned} &\frac{1}{N}\sum_m \cos^2(\theta_m) = \frac{1}{N}\sum_m \sin^2(\theta_m) = \frac{N}{2} \\ &\frac{1}{N}\sum_m \sin(\theta_m)\cos(\theta_m) = 0, \end{aligned} \tag{A3}$$

and we obtain

$$C(t) = \tfrac{1}{2}[\xi_1(t) + i\xi_2(t)]. \tag{A4}$$

For a spinning wave for example one has that $\xi_1(t) = \cos(\omega t)$ and $\xi_2(t) = \sin(\omega t)$, and one obtains

$$C(t) = \tfrac{1}{2}e^{i\omega t} \tag{A5}$$

for the case of equispaced pressure sensors. Indeed, one finds that the indicator has a phase that is linearly increasing in this case. If, however, the sensors are not equispaced, we now show that the indicator C is biased. In particular one obtains

$$\begin{aligned} &\frac{1}{N}\sum_m \xi_1 \cos^2(\theta_m) = \frac{N}{2}(1-\delta) \\ &\frac{1}{N}\sum_m \xi_1 \sin^2(\theta_m) = \frac{N}{2}(1+\delta) \\ &\frac{1}{N}\sum_m \xi_1 \sin(\theta_m)\cos(\theta_m) = \frac{N}{2}\mu. \end{aligned} \tag{A6}$$

By substituting (A6) into (A2) one obtains

$$C(t) = \left(\frac{1-\delta}{2} + \frac{\mu}{2}\right)\xi_1 + i\left(\frac{1+\delta}{2} + \frac{\mu}{2}\right)\xi_2. \tag{A7}$$

For a spinning wave one has that $\xi_1 = \cos(\omega t)$ and $\xi_2 = \sin(\omega t)$, and we obtain

$$C(t) = \left(\frac{1-\delta}{2} + \frac{\mu}{2}\right)\cos(\omega t) + i\left(\frac{1+\delta}{2} + \frac{\mu}{2}\right)\sin(\omega t). \tag{A8}$$

This is the parametrization of an ellipse in the (ξ_1, ξ_2) plane. As a result, the phase of the complex number C is still linked to the nature of the mode, but the slope depends on the time t in a way that depends on the frame of reference due to the unevenly spacing of the sensors. This is an unwanted feature, since the nature of the mode should be independent of the frame of reference. Moreover, the phase of C depends already on time even in the case of evenly spaced sensors, with an additional wavy pattern on top of the linear increase (or decrease), as exemplified in Fig. 8, Type 2, in Ref. [21].

APPENDIX B: STANDING AND SPINNING WAVES IN TERMS OF $\{A_1, A_2, \tilde{\varphi}\}$

We discuss in Appendix B 1 the case of standing waves and in Appendix B 2 the case of spinning waves.

1. Standing waves

If $A_1 = 0$ or $A_2 = 0$ by direct substitution in Eq. (5) one observes trivially that the pressure field is standing.

We then prove that if the phase $\tilde{\varphi}$ defined in Eq. (6) is 0 or π, the system exhibits a standing wave. We can substitute $\varphi_2 = \varphi_1 + k\pi$ into (5), for $k = 0, 1$. By substituting also the identity $\cos(\alpha + k\pi) = (-1)^k \cos(\alpha)$ into (5) we obtain

$$p(\theta, t) = [A_1(t)\cos(n\theta) + (-1)^k A_2 \sin(n\theta)]\cos[\omega t + \varphi_1(t)]. \tag{B1}$$

We can define the auxiliary amplitude A and angle $n\theta_0$ as

$$\begin{aligned} A &\equiv A_1^2 + A_2^2 \\ n\theta_0 &\equiv \mathrm{Arg}[A_1 + i(-1)^k A_2] \end{aligned} \tag{B2}$$

and the inverse transformation

$$\begin{aligned} A_1 &= A\cos(n\theta_0) \\ (-1)^k A_2 &= A\sin(n\theta_0). \end{aligned} \tag{B3}$$

Substituting (B3) into (B1) we obtain

$$p(\theta, t) = A(t)\cos[n(\theta - \theta_0)]\cos[\omega t + \varphi_1(t)]. \tag{B4}$$

We observe from (B4) that at all instants of time the mode shape is fixed to $\cos[n(\theta - \theta_0)]$, i.e., the system exhibits a pure standing mode with a pressure antinode at $\theta = \theta_0$.

2. Spinning waves

We now prove that if $A_1 = A_2$ and $\tilde{\varphi} = \pm\pi/2$ the system exhibits a spinning wave, rotating, respectively, in the counterclockwise and clockwise direction. From (6) we can calculate first $\varphi_2 = \varphi_1 \mp \pi/2$, and then substitute it into (5), together with $A_1 = A_2 = A$:

$$p(\theta, t) = A(t)\cos[\omega t + \varphi_1(t)]\cos(n\theta) + A(t)\cos[\omega t + \varphi_1(t) \mp \pi/2]\sin(n\theta). \tag{B5}$$

We now substitute the identity $\cos(\alpha \mp \pi/2) = \pm\sin(\alpha)$ into (B5) and obtain

$$p(\theta, t) = A(t)\cos[\omega t + \varphi_1(t)]\cos(n\theta) + A(t)\sin[\omega t + \varphi_1(t)]\sin(n\theta) \tag{B6}$$

$$= A(t)\cos[\omega t + \varphi_1(t) \mp n\theta]. \tag{B7}$$

We notice from (B7) that the system exhibits a rotating (spinning) wave, respectively, in the counterclockwise or clockwise direction.

APPENDIX C: CALCULATION OF A, θ_0, χ from ξ

This Appendix discusses how to calculate the slow variables $A, n\theta_0, \chi$ and the fast variable $\phi \equiv \omega t + \varphi$ as defined in Eq. (27) and presented again here:

$$\xi_a(t) = A(t) e^{in\theta_0(t)} e^{-k\,\chi(t)} e^{j\phi(t)} \tag{C1}$$

for a nonzero quaternion ξ_a.

Step 1. The amplitude A is by definition the modulus of the quaternion ξ_a, i.e., $A \equiv |\xi_a|$. One can then normalize the quaternion to obtain

$$\xi_a^\sharp \equiv \frac{\xi_a}{A} = a + ib + jc + kd. \tag{C2}$$

The nature angle χ is calculated as

$$\chi = \frac{\arcsin[2(bc - ad)]}{2}. \tag{C3}$$

Step 2. If $\chi = \pm\pi/4$ one sets

$$\begin{aligned} n\theta_0 &= 0 \\ \phi^\sharp &= \text{arctan2}[2(bd - ac), a^2 - b^2 - c^2 + d^2]/2. \end{aligned} \tag{C4a}$$

If instead $\chi \neq \pm\pi/4$ one sets instead

$$\begin{aligned} n\theta_0 &= \text{arctan2}[2(ab + cd), a^2 - b^2 + c^2 - d^2]/2 \\ \phi^\sharp &= \text{arctan2}[2(bd + ac), a^2 + b^2 - c^2 - d^2]/2, \end{aligned} \tag{C4b}$$

where $\phi^\sharp$ is a temporary variable that we need to further manipulate to obtain ϕ, and $\text{arctan2}(y, x)$ is the argument of the complex number $x + iy$ with codomain $(-\pi\ ,\ \pi]$.

Step 3. If $e^{in\theta_0 - k\chi + j\phi^\sharp} = -\xi_a^\sharp$:

$$\begin{aligned} &\text{if } \phi^\sharp \geqslant 0 \Rightarrow \text{set} \quad \phi = \phi^\sharp - \pi \\ &\text{else } \phi^\sharp < 0 \Rightarrow \text{set} \quad \phi = \phi^\sharp + \pi. \end{aligned} \tag{C5a}$$

If instead $e^{in\theta_0 - k\chi + j\phi^\sharp} = +\xi_a^\sharp$,

$$\text{set } \phi = \phi^\sharp. \tag{C5b}$$

The procedure discussed up to this point matches, apart for a typographical error corrected in Eq. (C4), the one presented by Flamant *et al.* [15]. It allows the reconstruction of the slow variables $A, n\theta_0, \chi$ that fully characterize the nature, orientation, and amplitude of the acoustic field, in the domains $A \in (0, \infty)$, $n\theta_0 \in (-\pi/2, \pi/2]$, $\chi \in [-\pi/4, \pi/4]$, $\phi \in (-\pi, \pi]$. This procedure, however, has a shortcoming when one applies it not to just to one fixed instant of time, but to a signal or time series $\xi_a(t)$. In particular, as we exemplify next, the reconstructed fast phase ϕ and the orientation angle $n\theta_0$ are not guaranteed to be continuous functions of the time t if the procedure above is applied.

We consider the case of $n\theta_0$ increasing from a value smaller than $\pi/2$, corresponding in Fig. 3 to an ellipse rotating counterclockwise with the major axis aligning with the vertical axis ξ_2. When the ellipse's major axis overtakes the vertical axis ξ_2 by an angle $\Delta\theta$ moving in the counterclockwise direction, the value of $n\theta_0$ is mapped from a positive value to the negative value $-\pi/2 + \Delta\theta$. This happens because indeed the angle of the major axis of the ellipse can be described both with the negative angle $-\pi/2 + \Delta\theta$ and with the positive angle $\pi/2 + \Delta\theta$. The procedure above chooses the value of $n\theta_0$ such that the domain of $n\theta_0$ is smallest and always calculates $n\theta_0$ in the range $(-\pi/2, \pi/2]$. This, however, has the shortcoming that every time the described scenario happens,

i.e., the major axis of the ellipse crosses the vertical axis ξ_2 in Fig. 3, the orientation angle $n\theta_0$ and the fast oscillating phase ϕ undergo a jump of π. This jump is not physical and compromises typical time series analyses techniques. To overcome this problem, we choose to reconstruct the orientation angle $n\theta$ as a continuous variable in the range $(-\pi, \pi]$.

In practice this requires to manipulate $n\theta$ after step 2 and before step 3, with an additional step 2b:

Step 2b. Let $n\theta_{0,m}$ be the value of $n\theta_0$ at the discrete instant of time t_m. For each time step t_m except the first at $m = 0$, we consider if $|n\theta_{0,m} - n\theta_{0,m-1}| > \pi/2$. If it is the case we calculate first

$$n\theta^{\sharp}_{0,m} = n\theta_{0,m} - \pi \,\mathrm{sign}(n\theta_{0,m} - n\theta_{0,m-1}) \tag{C6}$$

and then replace the value of $n\theta_{0,m}$ with $\mathrm{mod}(n\theta^{\sharp}_{0,m} + \pi, 2\pi) - \pi$, where $\mathrm{mod}(x, y)$ is the remainder of the division of x by y. Once this step is applied sequentially from $m = 1$ to the last time step, we proceed to step 3.

APPENDIX D: NATURE ANGLE χ AND SPIN RATIO s

From (9) we calculate $\xi_{\mathrm{a},1}$ and $\xi_{\mathrm{a},2}$ as functions of $\xi^{\pm}_{\mathrm{a}}$:

$$\begin{aligned} \xi_{\mathrm{a},1} &= \xi^{+}_{\mathrm{a}} + \xi^{-}_{\mathrm{a}} \\ \xi_{\mathrm{a},2} &= j(\xi^{-}_{\mathrm{a}} - \xi^{+}_{\mathrm{a}}). \end{aligned} \tag{D1}$$

We substitute (D1) into (20a) and obtain

$$\xi_{\mathrm{a}} = (1-k)\xi^{+}_{\mathrm{a}} + (1+k)\xi^{-}_{\mathrm{a}} = \sqrt{2}e^{-k\pi/4}\xi^{+}_{\mathrm{a}} + \sqrt{2}e^{+k\pi/4}\xi^{-}_{\mathrm{a}}. \tag{D2}$$

We express $\xi^{\pm}_{\mathrm{a}}$ in terms of their slowly varying amplitudes, similarly to (19), and substitute them in Eq. (D2):

$$\xi_{\mathrm{a}} = \sqrt{2}e^{-k\pi/4}A^{+}e^{j(\omega t+\varphi^{+})} + \sqrt{2}e^{+k\pi/4}A^{-}e^{j(\omega t+\varphi^{-})}. \tag{D3}$$

We now want to calculate A^{+} and A^{-} appearing in Eq. (D3) as functions of the nature angle χ in Eq. (27). In Eq. (27) we set $n\theta_0 = 0$:

$$\xi_{\mathrm{a}} = Ae^{-k\chi}e^{j(\omega t+\varphi)}, \tag{D4}$$

and we dropped the direct dependence on time t in Eq. (D4) for brevity. We can set $n\theta_0 = 0$ without any loss of generality since the amplitudes of the two counter-rotating spinning modes do not depend on the origin of the azimuthal frame of reference. By equating (D4) and (D3) we find

$$A^{+} = A\frac{\cos\chi + \sin\chi}{\sqrt{2}}, \tag{D5a}$$

$$A^{-} = A\frac{\cos\chi - \sin\chi}{\sqrt{2}}. \tag{D5b}$$

Finally substituting (D5) into the definition (3) of s we recover (32).

APPENDIX E: ORIENTATION ANGLE $n\theta_0$ AND PHASE $\hat{\phi}$

In this Appendix we prove that $n\theta_0$ matches $\hat{\phi}/2$. We write a solution in terms of spinning modes from (12) as

$$p(\theta, t) = \frac{A^{+}}{2}e^{i\varphi^{+}}e^{i(\omega t - n\theta)} + \frac{A^{-}}{2}e^{i\varphi^{-}}e^{i(\omega t + n\theta)} + \mathrm{c.c.} \tag{E1}$$

We now assume $A^+ \geqslant A^-$ (with the other case following similarly), with

$$A^+ = A^- + \Delta A, \quad \text{with } \Delta A \geqslant 0. \tag{E2}$$

We substitute (E2) into (E1) and obtain

$$p(\theta, t) = \frac{A^-}{2}(e^{i(\varphi^+ - n\theta)} + e^{i(\varphi^- + n\theta)})e^{i\omega t} + \frac{\Delta A}{2}e^{i(\varphi^+ - n\theta + \omega t)} + \text{c.c.} \tag{E3}$$

We now recast the two phases in terms of their difference and their sum

$$\begin{aligned} \varphi^+ &= (\omega^\sharp - \omega)t + \hat{\varphi}/2 \\ \varphi^- &= (\omega^\sharp - \omega)t - \hat{\varphi}/2, \end{aligned} \tag{E4}$$

where

$$\omega^\sharp \equiv \omega + \frac{\varphi^+ + \varphi^-}{2t} \tag{E5}$$

perturbs the frequency of oscillation ω. We substitute (E4) into (E3) and obtain

$$p(\theta, t) = \frac{A^-}{2}(e^{i(\hat{\varphi}/2 - n\theta)} + e^{-i(\hat{\varphi}/2 - n\theta)})e^{i\omega^\sharp t} + \frac{\Delta A}{2}e^{i(\hat{\varphi}/2 - n\theta + \omega^\sharp t)} + \text{c.c.} \tag{E6}$$

$$= A^- \cos(\hat{\varphi}/2 - n\theta)e^{i\omega^\sharp t} + \frac{\Delta A}{2}e^{i(\hat{\varphi}/2 - n\theta + \omega^\sharp t)} + \text{c.c.}$$

$$= 2A^- \cos\left(n\theta - \frac{\hat{\varphi}}{2}\right)\cos(\omega^\sharp t) + \Delta A \cos\left(\frac{\hat{\varphi}}{2} - n\theta + \omega^\sharp t\right). \tag{E7}$$

The first and second terms in Eq. (E7) are respectively the standing and the spinning components of the pressure field, as in Eq. (35). By direct comparison with (35), we find that $\hat{\phi}/2$ matches the orientation angle $n\theta_0$.

[1] W. Krebs, G. Walz, P. Flohr, and S. Hoffmann, Modal Analysis of Annular Combustors: Effect of Burner Impedance, in *Proc. ASME Turbo Expo 2001* (ASME, New Orleans, LA, 2001), pp. 1–8.

[2] J. Lepers, W. Krebs, B. Prade, P. Flohr, G. Pollarolo, and A. Ferrante, Investigation of thermoacoustic stability limits of an annular gas turbine combustor test-rig with and without Helmholtz-resonators, in *Proc. ASME Turbo Expo 2005* (ASME, Reno-Tahoe, NV, 2005), pp. 1–13.

[3] M. R. Bothien, N. Noiray, and B. Schuermans, Analysis of azimuthal thermoacoustic modes in annular gas turbine combustion chambers, in *Proc. ASME Turbo Expo 2014* (ASME, Düsseldorf, 2014), pp. 1–11.

[4] J. O'Connor, S. Natarajan, M. Malanoski, and T. Lieuwen, Disturbance Field Characteristics of a Transversely Excited Annular Jet, in *Proc. ASME Turbo Expo 2010* (ASME, Glasgow, 2010), pp. 23–38.

[5] J. Schwing, F. Grimm, and T. Sattelmayer, A Model for the Thermo-Acoustic Feedback of Transverse Acoustic Modes and Periodic Oscillations in Flame Position in Cylindrical Flame Tubes, in *Proc. ASME Turbo Expo 2012* (ASME, Copenhagen, 2012), p. 14.

[6] G. Ghirardo, C. Di Giovine, J. P. Moeck, and M. R. Bothien, Thermoacoustics of can-annular combustors, J. Eng. Gas Turbines Power **141**, 011007 (2018).

[7] J. P. Moeck, M. Paul, and C. O. Paschereit, Thermoacoustic instabilities in an annular Rijke tube, in *Proc. ASME Turbo Expo 2010* (ASME, Glasgow, 2010), pp. 1219–1232.

[8] N. Noiray, M. R. Bothien, and B. Schuermans, Investigation of azimuthal staging concepts in annular gas turbines, Combust. Theory Modell. **15**, 585 (2011).

[9] M. Bauerheim, M. Cazalens, and T. Poinsot, A theoretical study of mean azimuthal flow and asymmetry effects on thermo-acoustic modes in annular combustors, Proc. Combust. Inst. **35**, 3219 (2015).

[10] G. Ghirardo, F. Boudy, and M. R. Bothien, Amplitude statistics prediction in thermoacoustics, J. Fluid Mech. **844**, 216 (2018).

[11] L. Crocco, Research on combustion instability in liquid propellant rockets, Symp. (Intl.) Comb. **12**, 85 (1969).
[12] G. Ghirardo and M. P. Juniper, Azimuthal instabilities in annular combustors: Standing and spinning modes, Proc. R. Soc. London A **469**, 20130232 (2013).
[13] G. Ghirardo, M. P. Juniper, and J. P. Moeck, Weakly nonlinear analysis of thermoacoustic instabilities in annular combustors, J. Fluid Mech. **805**, 52 (2016).
[14] N. Noiray and B. Schuermans, On the dynamic nature of azimuthal thermoacoustic modes in annular gas turbine combustion chambers, Proc. R. Soc. London A **469**, 20120535 (2013).
[15] J. Flamant, N. Le Bihan, and P. Chainais, Time-frequency analysis of bivariate signals, Appl. Comput. Harmonic Anal. **1**, 1 (2017).
[16] J. Flamant, N. Le Bihan, and P. Chainais, Spectral Analysis of Stationary Random Bivariate Signals, IEEE Trans. Signal Proc. **65**, 6135 (2017).
[17] T. Bulow and G. Sommer, Hypercomplex signals—A novel extension of the analytic signal to the multidimensional case, IEEE Trans. Signal Proc. **49**, 2844 (2001).
[18] B. Schuermans, C. O. Paschereit, and P. Monkewitz, Non-Linear Combustion Instabilities in Annular Gas-Turbine Combustors, in *44th AIAA Aerospace Sciences Meeting and Exhibit* (American Institute of Aeronautics and Astronautics, Reno, NV, 2006), pp. 1–12.
[19] P. M. Morse and K. U. Ingard, *Theoretical Acoustics* (Princeton University Press, Princeton, 1968).
[20] M. L. Munjal, *Acoustics of Ducts and Mufflers* (John Wiley & Sons, Bangalore, India, 1987).
[21] T. Poinsot, P. Wolf, G. Staffelbach, L. Y. M. Gicquel, and J. D. Muller, Annual Research Briefs, Center for Turbulence Research, Technical report, Center for Turbulence Research, Stanford University (2011).
[22] N. A. Worth and J. R. Dawson, Modal dynamics of self-excited azimuthal instabilities in an annular combustion chamber, Combust. Flame **160**, 2476 (2013).
[23] J.-F. Bourgouin, D. Durox, J. P. Moeck, T. Schuller, and S. Candel, Self-sustained instabilities in an annular combustor coupled by azimuthal and longitudinal acoustic modes, in *Proc. ASME Turbo Expo 2013* (ASME, San Antonio, TX, 2013), pp. 1–13.
[24] S. Evesque, W. Polifke, and C. Pankiewitz, Spinning and Azimuthally Standing Acoustic Modes in Annular Combustors, in *9th AIAA/CEAS Aeroacoustics Conf. and Exhibit* (AIAA, Hilton Head, SC, 2003), pp. 1–8.
[25] N. A. Worth and J. R. Dawson, Effect of equivalence ratio on the modal dynamics of azimuthal combustion instabilities, Proc. Combust. Inst. **36**, 3743 (2017).
[26] K. Prieur, D. Durox, T. Schuller, and S. Candel, Strong Azimuthal Combustion Instabilities in a Spray Annular Chamber with Intermittent Partial Blow-Off, J. Eng. Gas Turbines Power **140**, 031503 (2017).
[27] J.-F. Bourgouin, D. Durox, J. P. Moeck, T. Schuller, and S. Candel, Characterization and Modeling of a Spinning Thermoacoustic Instability in an Annular Combustor Equipped with Multiple Matrix Injectors, J. Eng. Gas Turbines Power **137**, 021503 (2015).
[28] D. Laera, T. Schuller, K. Prieur, D. Durox, S. M. Camporeale, and S. Candel, Flame Describing Function analysis of spinning and standing modes in an annular combustor and comparison with experiments, Combust. Flame **184**, 136 (2017).
[29] D. Gabor, Theory of communication, J. Inst. Electr. Eng. **93**, 429 (1946).
[30] J. Ville, Théorie et Applications de la Notion de Signal Analytique (translated in English by Michael D. Godfrey in February 2017), Cables Transmissions **2**, 61 (1948).
[31] B. Picinbono, On instantaneous amplitude and phase of signals, IEEE Trans. Signal Proc. **45**, 552 (1997).
[32] D. Rouwenhorst, J. Hermann, and W. Polifke, Online Monitoring of Thermoacoustic Eigenmodes in Annular Combustion Systems Based on a State-Space Model, J. Eng. Gas Turbines Power **139**, 1 (2017).
[33] T. Hummel, F. Berger, B. Schuermans, and T. Sattelmayer, Theory and Modeling of Non-Degenerate Transversal Thermoacoustic Limit Cycle Oscillations, in *Intl. Symp.: Thermoacoustic Instabilities in Gas Turbines and Rocket Engines* (Munich, 2016), pp. 1–13.
[34] W. R. Hamilton, On Quaternions; or on a new System of Imaginaries in Algebra, Letter to John T. Graves (1843), https://www.maths.tcd.ie/pub/HistMath/People/Hamilton/OnQuat/OnQuat.pdf.
[35] J. Gonella, A rotary-component method for analysing meteorological and oceanographic vector time series, Deep Sea Res. Ocean. Abst. **19**, 833 (1972).

[36] P. J. Schreier and L. L. Scharf, *Statistical Signal Processing of Complex-Valued Data* (Cambridge University Press, Cambridge, 2010).
[37] C. Doran and A. Lasenby, *Geometric Algebra for Physicists* (Cambridge University Press, Cambridge, 2003).
[38] N. Le Bihan, S. J. Sangwine, and T. A. Ell, Instantaneous frequency and amplitude of orthocomplex modulated signals based on quaternion Fourier transform, Signal Process. **94**, 308 (2013).
[39] By keeping the slowly varying quantities $a, \Delta, \delta, \theta_0, \varphi$ constant in the limit cycle; see, e.g., discussion around (19) in Ref. [44].
[40] A. Pikovsky, M. Rosenblum, and J. Kurths, *Synchronization* (Cambridge University Press, Cambridge, 2001).
[41] A. Balanov, N. Janson, D. Postnov, and O. Sosnovtseva, *Synchronization: From Simple to Complex* (Springer, Berlin, 2009).
[42] One needs to compare the expressions $\{A\cos\chi, A\sin\chi, n\theta_0, \omega t+\varphi\}$ of (36) with the expressions $\{a, b, \theta, \phi\}$ in (18) of Ref. [44].
[43] J. M. Lilly and J.-C. Gascard, Wavelet ridge diagnosis of time-varying elliptical signals with application to an oceanic eddy, Nonlinear Proc. Geophys. **13**, 467 (2006).
[44] J. M. Lilly and S. C. Olhede, Bivariate Instantaneous Frequency and Bandwidth, IEEE Trans. Signal Proc. **58**, 591 (2010).
[45] C. N. K. Mooers, A technique for the cross spectrum analysis of pairs of complex-valued time series, with emphasis on properties of polarized components and rotational invariants, Deep Sea Res. Ocean. Abst. **20**, 1129 (1973).
[46] R. C. Jones, A New Calculus for the Treatment of Optical Systems. Description and Discussion of the Calculus, J. Opt. Soc. Am. **31**, 488 (1941).
[47] H. Poincaré, Théorie mathématique de la lumière, Technical report, Faculté des sciences de Paris, Cours de Physique Mathématique (1887).
[48] To be fully accurate, Poincaré chose the angle $n\theta_0$ in Eq. (27) in the domain $[-\pi/2, \pi/2]$ instead of $[-\pi, \pi]$, and used twice the angle $n\theta_0$ as longitude coordinate. This difference is just a technical detail and is discussed towards the end of Appendix C.
[49] Indeed, when the system is purely spinning either clockwise or anticlockwise the angle $n\theta_0$ is undetermined, in the same manner that at the north and south poles of the sphere the latitude is undetermined.
[50] D. D. Holm, *Geometric Mechanics—Part I: Dynamics and Symmetry*, 2nd ed. (Imperial College Press, London, 2011).
[51] R. P. Feynman, F. L. Vernon, and R. W. Hellwarth, Geometrical Representation of the Schrödinger Equation for Solving Maser Problems, J. Appl. Phys. **28**, 49 (1957).
[52] R. P. Feynman, R. B. Leighton, and M. Sands, *The Feynman Lectures on Physics, Vol. III: Quantum Mechanics* (Basic Books, New York, 2011).
[53] J. P. Lowe and K. A. Peterson, *Quantum Chemistry*, 3rd ed. (Elsevier, Amsterdam, 2006).
[54] P. J. Schreier, Polarization ellipse analysis of nonstationary random signals, IEEE Trans. Signal Proc. **56**, 4330 (2008).
[55] P. Rubin-Delanchy and A. T. Walden, Kinematics of complex-valued time series, IEEE Trans. Signal Proc. **56**, 4189 (2008).
[56] S. Chandna and A. T. Walden, Simulation methodology for inference on physical parameters of complex vector-valued signals, IEEE Trans. Signal Proc. **61**, 5260 (2013).
[57] Technically, these are marginal bivariate PDFs, obtained from the trivariate PDF of the state of the system by marginalizing over one of the three variables.
[58] Projected either on two orthogonal standing modes as in Sec. III A or on two counter-rotating modes as in Sec. III B.
[59] G. Rigas, A. R. Oxlade, A. S. Morgans, and J. F. Morrison, Low-dimensional dynamics of a turbulent axisymmetric wake, J. Fluid Mech. **755**, R51 (2014).
[60] G. Rigas, L. Esclapez, and L. Magri, Proceedings of the Summer Program 2017 of the Center for Turbulence Research, Technical report, Center for Turbulence Research. Stanford University (2016), arXiv:1703.07405.